SCIENTIFIC REP⚙RTS

Non-uniform Solute Segregation at Semi-Coherent Metal/Oxide Interfaces

Samrat Choudhury[1,#], Jeffery A. Aguiar[1,†], Michael J. Fluss[2], Luke L. Hsiung[2], Amit Misra[1,*] & Blas P. Uberuaga[1]

The properties and performance of metal/oxide nanocomposites are governed by the structure and chemistry of the metal/oxide interfaces. Here we report an integrated theoretical and experimental study examining the role of interfacial structure, particularly misfit dislocations, on solute segregation at a metal/oxide interface. We find that the local oxygen environment, which varies significantly between the misfit dislocations and the coherent terraces, dictates the segregation tendency of solutes to the interface. Depending on the nature of the solute and local oxygen content, segregation to misfit dislocations can change from attraction to repulsion, revealing the complex interplay between chemistry and structure at metal/oxide interfaces. These findings indicate that the solute chemistry at misfit dislocations is controlled by the dislocation density and oxygen content. Fundamental thermodynamic concepts – the Hume-Rothery rules and the Ellingham diagram – qualitatively predict the segregation behavior of solutes to such interfaces, providing design rules for novel interfacial chemistries.

Metal/oxide composite structures are ubiquitous in technology with applications including microelectronics[1], magnetoresistance devices[2], thermal barriers[3], nanocatalysts[4], and structural materials for nuclear reactors[5]. The macroscopic properties of metal/oxide composites are often driven by the structure and chemistry at the metal/oxide interface (MOI). Solutes are often added to the metal to improve various properties, such as adhesion of the metal/oxide interface[6] and corrosion resistance[7]. However, solute segregation to the metal/oxide interfaces can drastically alter atomic and electronic structure, microstructure, chemistry and macroscopic properties of the interface. For example, at the microstructural scale segregation of Sb to Ag/Mn_3O_4 interfaces alters the morphology of Mn_3O_4 precipitates[8], which in-turn prevents precipitate coarsening. Experimental evidence also shows that segregation of Cu to Ni/Cr_2O_3 interfaces improves corrosion resistance in Ni-based alloys[9]. Hence, an ability to predict solute segregation tendencies to metal/oxide interfaces is critical in designing novel metal/oxide composites with optimum properties.

Solute segregation to metal/oxide interfaces is governed by two competing energetic contributions: chemical and strain energy. Except in a few cases[10–12], where the electronic structure at the metal/oxide interface was discussed, literature studies have relied upon the elastic strain energy due to size mismatch between the metal and the solute to interpret segregation to metal/oxide interfaces[13,14], which works reasonably well for solutes that do not interact significantly with the oxide. For example, Sebastian et al.[15] observed that the relative segregation of solutes such as antimony and silver to the MgO/Cu interface correlates with the elastic strain energy arising from the size mismatch between the solutes and copper. However, in the same work, this approach failed to explain the high segregation of Au to CdO/Ag interfaces, where the strain energy is negligible.

[1]Los Alamos National Laboratory, Los Alamos NM 87545. [2]Lawrence Livermore National Laboratory, Livermore, California 94551, USA. *Present address: University of Michigan, Ann Arbor, MI 48109. #Present address: University of Idaho, Moscow, ID 83844. †Present address: National Renewable Energy Laboratory, Golden, CO 80401. Correspondence and requests for materials should be addressed to S.C. (email: metsam4@yahoo.com)

The prediction of segregation to semi-coherent interfaces i.e. with misfit dislocations is even more complex. Misfit dislocations are separated by patches of coherent regions (terraces) with maximum coincidence. The misfit dislocations at metal/oxide interfaces have strain fields surrounding the dislocation, as in metallic composites, but also exhibit a significantly different localized chemistries than the terraces[16]. The combination of the in-plane variation of the strain field and the variable chemistry surrounding a misfit dislocation can lead to drastically different (up to 50 times) segregation of solutes between the terrace and the misfit region in a metal/ceramic interface[17]. Further, it has been observed that S and Ag segregate to the NiAl/Al$_2$O$_3$[7] and MgO/Cu[13] interfaces, respectively, as the oxide particle grows because the interface loses coherency with particle size, forming misfit dislocations.

Thus, while the strain energy due to size mismatch between the solute and the matrix can provide qualitative insight into segregation tendencies at grain boundaries in metals[18], the strain energy alone cannot explain solute segregation at metal/oxide interfaces. Such considerations will not be adequate for solutes with strong oxide-forming tendencies. In particular, as shown in Ref. 16 under oxidizing conditions the local oxygen content at the interface varies dramatically between the misfit and coherent region of a metal/oxide interface. Previously, researchers have observed that the electronic structure at a metal/oxide interface is dependent on the local atomic arrangement[11]. In this paper, we show that, under oxidizing conditions, the non-uniform oxygen content at the interface, especially the presence of oxygen in the misfit region of the interface can lead to dramatically distinct segregation behavior between the misfit and the coherent region of a metal/oxide interface. We present electronic structure calculations of solute segregation at a metal/oxide interface containing misfit dislocations using Fe/Y$_2$O$_3$ as a model system. Fe/Y$_2$O$_3$ is chosen as a surrogate for the more complex Y-Ti-O oxide particles within nanostructured ferritic alloys (NFAs)[5], a potential candidate structural material for next-generation nuclear reactors. However, our results have broader implications for metal/oxide interfaces more generally.

To emphasize the chemical contribution towards solute segregation tendencies, we choose solutes with a wide range of oxide forming tendencies, but relatively minimal atomic size mismatch (<10%) with iron. The tendency of a solute to form an oxide was obtained from the Ellingham diagram[19], a plot of the free energy of oxide formation versus temperature and oxygen partial pressure (p_{O2}). We show that the local oxygen environment and the oxide-forming tendency of the solute govern segregation of the solute to particular iron sites at the Fe/Y$_2$O$_3$ interface. We verify our predicted behavior with electron energy loss spectroscopy (EELS)-measured Cr segregation in a nanostructured ferritic alloy. Finally, we generalize our results using Hume-Rothery rules and the Ellingham diagram to provide insight into solute segregation at arbitrary metal/ceramic interfaces.

Results

To study the solute segregation behavior at a metal/oxide interface we created a bi-layer supercell of Fe/Y$_2$O$_3$ (see the Method Section for a description of the supercell geometry). Electronic structure calculations were performed to calculate the segregation energies of solutes using the Vienna *ab-initio* Simulation Package (VASP)[20,21]. We first present the as-calculated segregation tendencies of solutes at the coherent terraces of the Fe/Y$_2$O$_3$ interface. Starting with the DFT-calculated relaxed structure of the ideal Fe/Y$_2$O$_3$ interface, we replaced a Fe atom within the terrace of the interfacial Fe layer with a solute atom and allowed the system to relax again. Similar calculations were performed in bulk Fe. The segregation energy of the solute to the Fe/Y$_2$O$_3$ interface is:

$$E^{Seg} = (E^{Interface}_{with\ solute} - E^{Interface}_{without\ solute}) - (E^{bulk}_{with\ solute} - E^{bulk}_{without\ solute}) \qquad (1)$$

In Eq. (1) entropic contributions are not considered. We expect the qualitative segregation tendencies we predict will not be affected by the entropic contributions[22]. Based on Eq. (1), a negative segregation energy indicates the solute prefers to segregate to the interface, while a positive segregation energy means the solute prefers to reside in the bulk bcc Fe matrix. Based on the Ellingham diagram, two sets of substitutional solutes[23] were considered: (i) solutes (Cr, Al, Mg) with a stronger oxide forming tendency than Fe; (ii) solutes (Co, Ni, Cu) with a weaker oxide forming tendency than Fe.

To understand the role of chemical interactions between the solute and oxygen on the segregation energy of the solute, we systematically inserted 1-3 oxygen atoms at interstitial sites (mid-point between the solute and the neighboring Fe atom) within the interfacial iron layer at the terrace and allowed the system to relax. The segregation energy of the solute as a function of oxygen interstitial content was calculated using an expression similar to Equation (1) with the terms in the first bracket corresponding to the energies of the supercell with/without the solute in the presence of oxygen interstitials. We note that these segregation energies are independent of oxygen chemical potentials.

Figure 1(a–d) show plan views of the terrace in the Fe/Y$_2$O$_3$ interface with increasing oxygen content surrounding the solute (Cr in this case). The segregation energies of various solutes with increasing number of oxygen interstitials are presented in Fig. 1(e,f). Two distinct trends are observed. For solutes with weaker oxide forming tendencies than iron, segregation energies decrease as the oxygen content at the interface increases (Fig. 1(e)). Further, the change in segregation energy of the solute per oxygen interstitial ($\Delta E^{Seg}_{Cu} > \Delta E^{Seg}_{Ni} > \Delta E^{Seg}_{Co}$) is inversely related to the free energy of oxide formation of the respective solutes obtained from the Ellingham diagram[19] (i.e. weaker oxide-formers are more repelled by the interface). In the case of Co, the segregation energy switches from negative to positive with
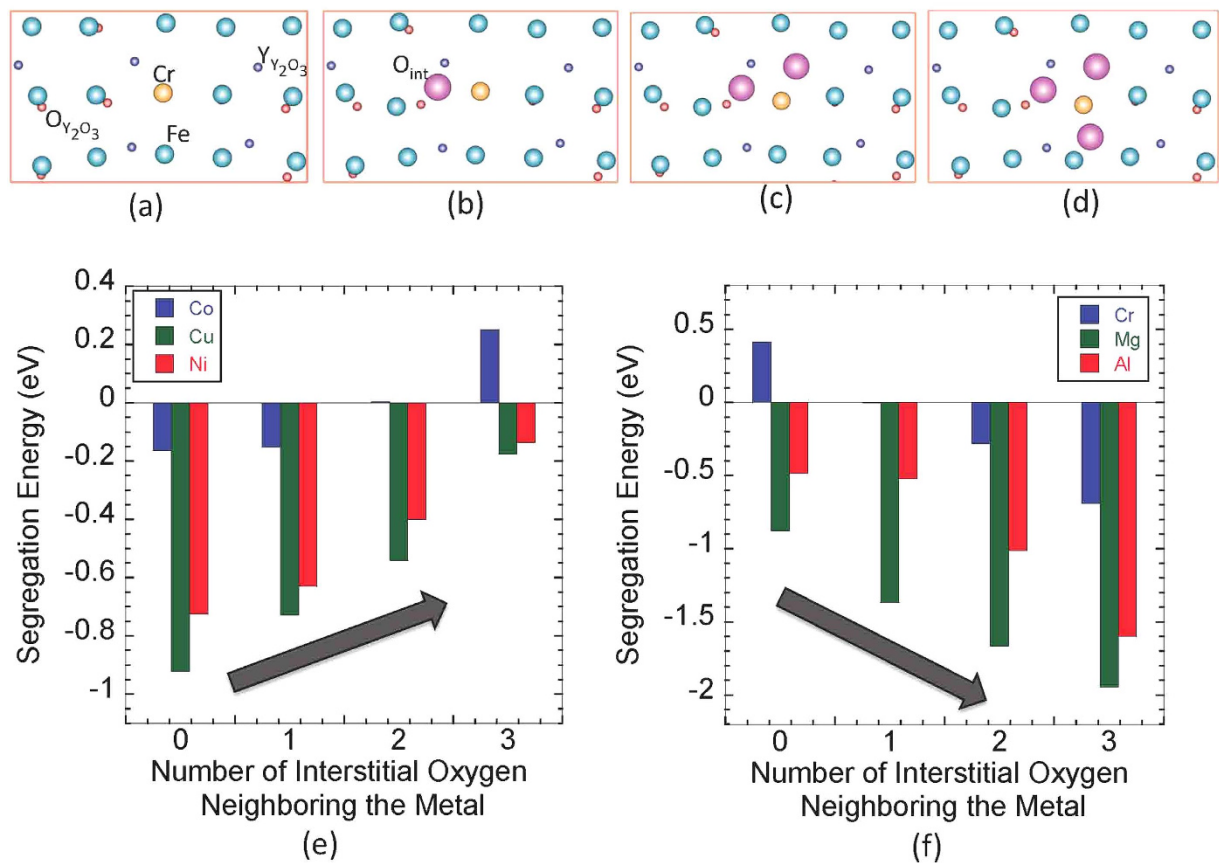
Figure 1. (**a–d**) Planar view of atoms for a selected potion of the Fe/Y_2O_3 interface obtained from electronic structure calculations with increasing number of interstitial oxygen surrounding a Cr atom. In these plots iron, chromium and interstitial oxygen within the interfacial iron layer are represented by green, orange and pink circles, while the small blue and red circles represent yttrium and oxygen atoms within the interfacial yttria layer. (**e,f**) Segregation energy of solutes with increasing number of interstitial oxygen surrounding the solute: (**e**) solutes with weaker oxidizing tendencies than iron; (**f**) solutes with stronger oxidizing tendencies than iron.

increasing oxygen content implying that Co is repelled by the interface under an oxidizing environment at the interface, but is attracted under reducing conditions.

The opposite trend in segregation behavior is observed for strong oxide formers such as Cr, Al and Mg (Fig. 1(f)). The role of oxygen at grain boundaries and heterointerfaces on the segregation of strong oxide-forming elements has also been observed experimentally. Williams *et al.*[24] observed that the segregation and subsequent formation of oxides of Cr at grain boundaries in NFAs is preceded by the segregation of oxygen. Similarly, segregation of strong oxide forming elements like Cr and V to the Fe/Y_2O_3 interface has been observed from atom-probe tomography, correlating with excess oxygen at the interface[25].

Based on these results, we conclude that the propensity of these solutes to segregate to the terraces at the interface can be controlled by varying the interfacial oxygen content with different terminating layer (O or metal)[26,27], which in turn can be controlled by varying p_{O2}. Further, we observe that, in the absence of interstitial oxygen, the segregation energies of the various solutes to the coherent terraces follow Hume-Rothery rules[28]. Hume-Rothery rules provide a simple description of the tendency of a solute to dissolve in a solvent/matrix based on the mismatch of crystal structures, atomic radius, electronegativity and valency between the solute and solvent. All of the solutes considered, with the exception of Cr, have a different crystal structure than the bcc Fe matrix; hence all segregate to the interface. In contrast, Cr, which is bcc in nature, is more stable in the bulk Fe matrix, consistent with experimental observations that Cr prefers to reside in bulk Fe rather than segregating to the surface[29]. Thus, it is possible to predict the solute segregation tendency in absence of interstitial oxygen based on selected Hume-Rothery rules. We note that, to reduce the complexity of the comparisons, the present study was limited to solutes with similar atomic radii and electronegativities (except Mg) as Fe.
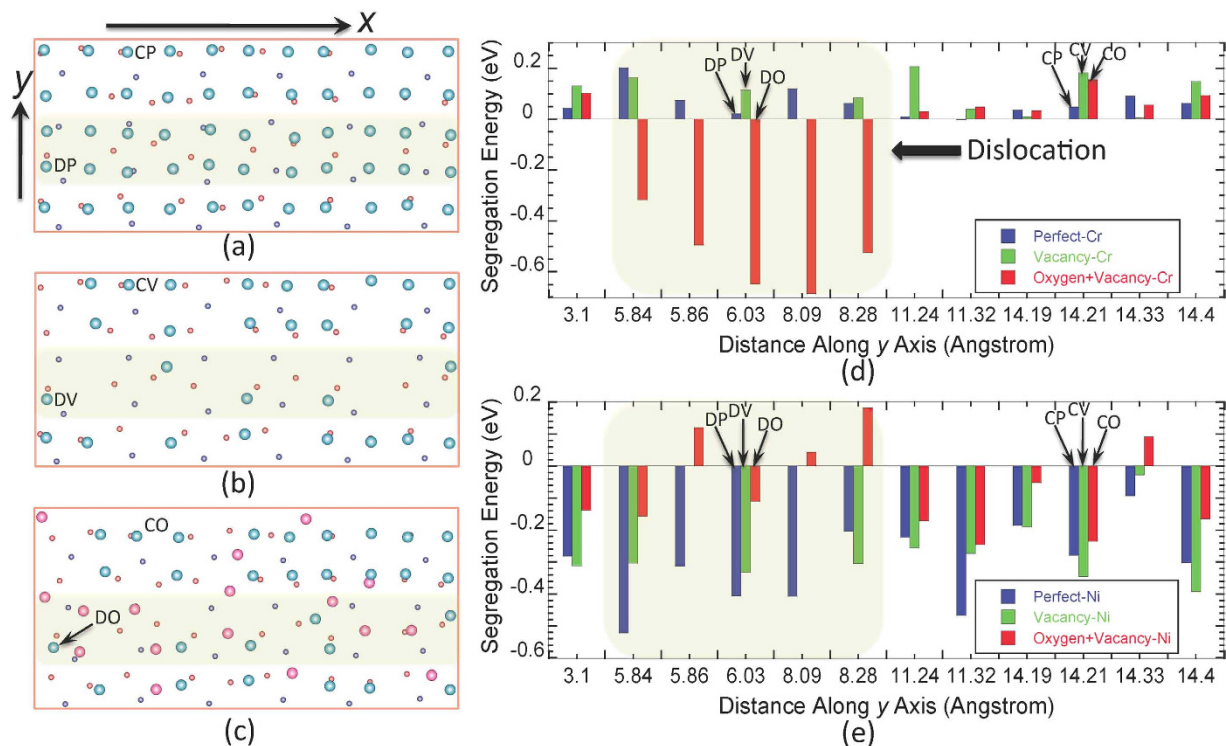
Figure 2. **(a–c)** Planar view of Fe atoms (green), interstitial O atoms (pink), O atoms in Y_2O_3 (small red) and Y atoms in Y_2O_3 (blue) at the Fe/Y_2O_3 interface obtained from electronic structure calculations: **(a)** relaxed structure of the initial as-constructed interface; **(b)** Fe vacancy stabilized structure; **(c)** combined oxygen interstitial and Fe vacancy stabilized structure. **(d–f)** Spatial variation of Cr and Ni segregation energies within the dislocation and coherent regions. In all the figures, the shaded yellow region represents the dislocation. The Fe atomic sites along the y-direction are separated uniformly, not by real positions. In the bar charts in (e) and (f), blue, green and red refer to perfect (P), Fe vacancy-stabilized (V) and oxygen interstitial + Fe vacancy stabilized (O) interfaces, respectively; sites referred to in the text are labeled as DP, DV, DO and CP, CV, CO respectively in the dislocation (D) core and coherent (C) regions of the interface.

Thus, within the interfacial terraces, the segregation tendencies of the various solutes strongly depend on the local oxygen content. We have shown previously that the local oxygen content at the interface changes dramatically from the terraces to the misfit regions[16]. We thus expect very different segregation behavior at the misfit dislocations as compared to the terrace. Figure 2(a) shows a planar view of the interfacial iron and yttria layer of the relaxed Fe/Y_2O_3 interface[16]. In the y direction, there are five atomic columns of iron for every 4 atomic columns of oxygen in the Y_2O_3 layer leading to the formation of a misfit dislocation (shaded region) accommodating the lattice mismatch and a chemical imbalance (high Fe/O ratio ~2) in the neighborhood of the misfit dislocation as compared to in the terrace (Fe/O ratio ~1) that destabilizes the structure. The structure can be stabilized by either introducing Fe vacancies (Fig. 2b) or a combination of Fe vacancies and oxygen interstitials (Fig. 2c), depending on the oxygen content[16]. Importantly, the vast majority of these stabilizing point defects reside within the dislocation region, indicating that the local chemistry at the misfit dislocation is very different than at the terraces. We calculated the segregation energies for Cr and Ni at selected interfacial iron sites across the interface (both in the terrace and misfit regions) within the initial or perfect (no point defects) Fe/Y_2O_3 interface, the Fe vacancy-stabilized structure, and the combined Fe vacancy + oxygen interstitial-stabilized structure (Fig. 2(d,e)). As shown in Fig. 2d, for the structures corresponding to Fig. 2a,b, Cr is repelled by the interface. The repulsion is stronger for sites within the misfit region as they have a reduced oxygen environment (high Fe/O ratio). However, under oxidizing conditions, when both Fe vacancies and interstitial oxygen are present in the misfit region (Fig. 2c), Cr strongly segregates to the misfit dislocation. The Cr segregation tendency within the terrace remains relatively unchanged within the three structures. The opposite tendencies are observed in the case of Ni (Fig. 2e). Ni, an fcc element, prefers to segregate to the interface within the perfect and the Fe vacancy-stabilized interfaces. However, under oxidizing conditions Ni, which is a weaker oxide former than Fe, experiences some repulsion by the interface, particularly at the misfit region. This is consistent with our observation for segregation to the terrace as a function of oxygen content (Fig. 1e).
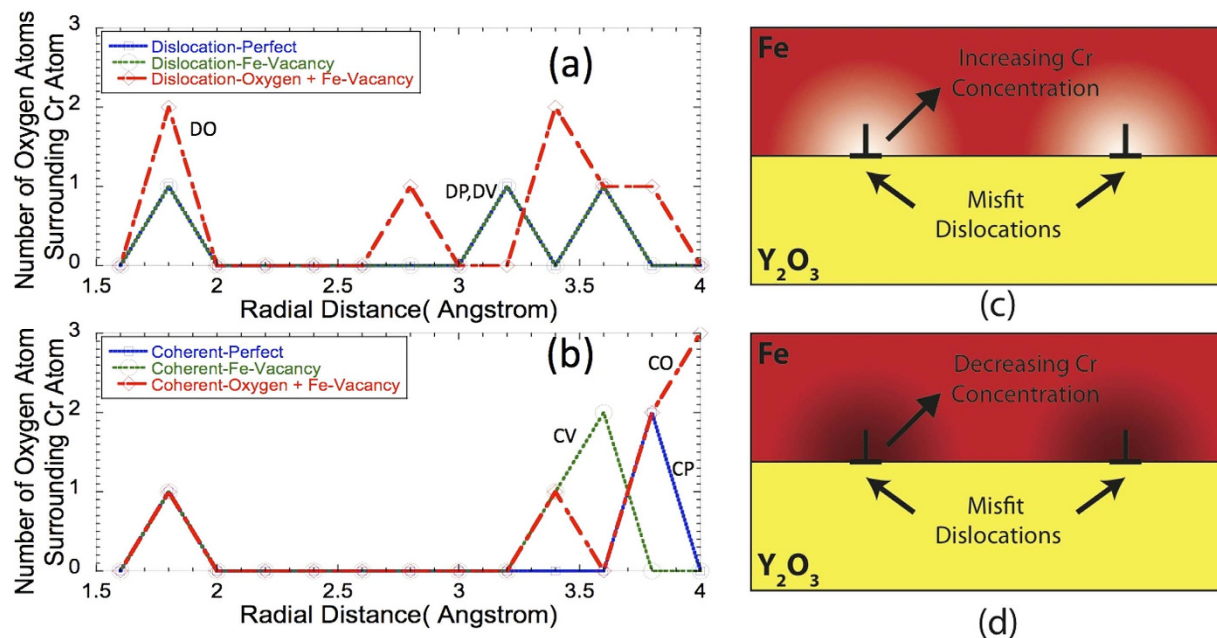
Figure 3. (a,b) Distribution of the total number of oxygen atoms (interstitial O and O in Y_2O_3) surrounding the solute (Cr, Ni) at the sites presented in Fig. 2(a–c): **(a)** sites within the dislocation region; **(b)** sites within the coherent region. **(c,d)** Schematic concentration profile of Cr at the Fe/Y_2O_3 interface with two misfit dislocations. The hue of red at the interface represents the Cr concentration, i.e. darker red implies higher Cr concentration. **(c)** Cr concentration under oxygen-poor/reducing conditions; **(d)** Cr concentration under oxygen-rich/oxidizing conditions.

Figures 3(a,b) demonstrate quantitatively the role of oxygen on Cr segregation tendencies. The oxygen chemical environment is described in terms of the number of oxygen as a function of radial distance surrounding a Cr atom. In calculating the number of oxygen surrounding the solute, both interstitial oxygen and oxygen within the interfacial yttria layer were counted. Two representative sites, C (within the terrace) and D (within the misfit dislocation), within the three structures – perfect (P), iron vacancy-stabilized structure (V) and iron vacancy + oxygen interstitial-stabilized structures (O) – were considered. Fig. 3(a,b) shows that the oxygen environment for Cr up to distances of 2.5 Å is identical except for the iron site (DO) in the O structure. For this site, Cr has additional oxygen in close proximity, explaining the observed segregation tendency in Fig. 2(d). Based on the calculated segregation behavior, a schematic of the Cr concentration profile at the interface with misfit dislocations is presented in Fig. 3(c,d) for two scenarios. Under reducing conditions (Fig. 3c), no Cr atoms are expected at the misfit dislocation. The Cr concentration in a Fe-Cr alloy will increase from zero at the misfit dislocation to bulk Cr concentration with increasing distance from the interface. However, under oxidizing conditions the maximum Cr concentration is expected precisely at the misfit dislocation core (Fig. 3d). Thus it can be concluded that the solute concentration at the misfit region is a strong function of the local oxygen content.

To verify our predicted enrichment of Cr concentration tendencies at the misfit dislocations, we performed STEM and STEM-based EELS imaging of an embedded $YAl_xCr_{1-x}O_3$ particle within a ferritic matrix (Fig. 4a). Fig. 4b indicates the semi-coherent nature of the interface using selected area diffraction. Fig. 4c shows STEM-EELS point-to-point line scans resolving the chemical profiles for Cr traversing an interfacial dislocation and a coherent terrace. Comparing the chemical profiles, we note the increased segregation of Cr to the dislocation in stark contrast to the terrace. Although the enrichment of Cr at the misfit region is not uniform, experimentally we observed that there is an overall increased abundance of Cr to the misfit region of the metal/oxide interface compared to the coherent terraced regions, which agrees qualitatively with our theoretical predictions.

Discussion

Our results provide two parameters, dislocation density and local oxygen content (or p_{O2}), to tailor the solute chemistry at metal/oxide interfaces. Further, we have shown that thermodynamic concepts – Hume-Rothery rules and the Ellingham diagram – can provide qualitative insight regarding the relative segregation tendencies of different solutes (via the Hume-Rothery rules) and the preferential segregation sites at the interface (via the Ellingham diagram, provided the oxygen structure at the interface is known). However, the oxygen distribution at the interface necessary to predict
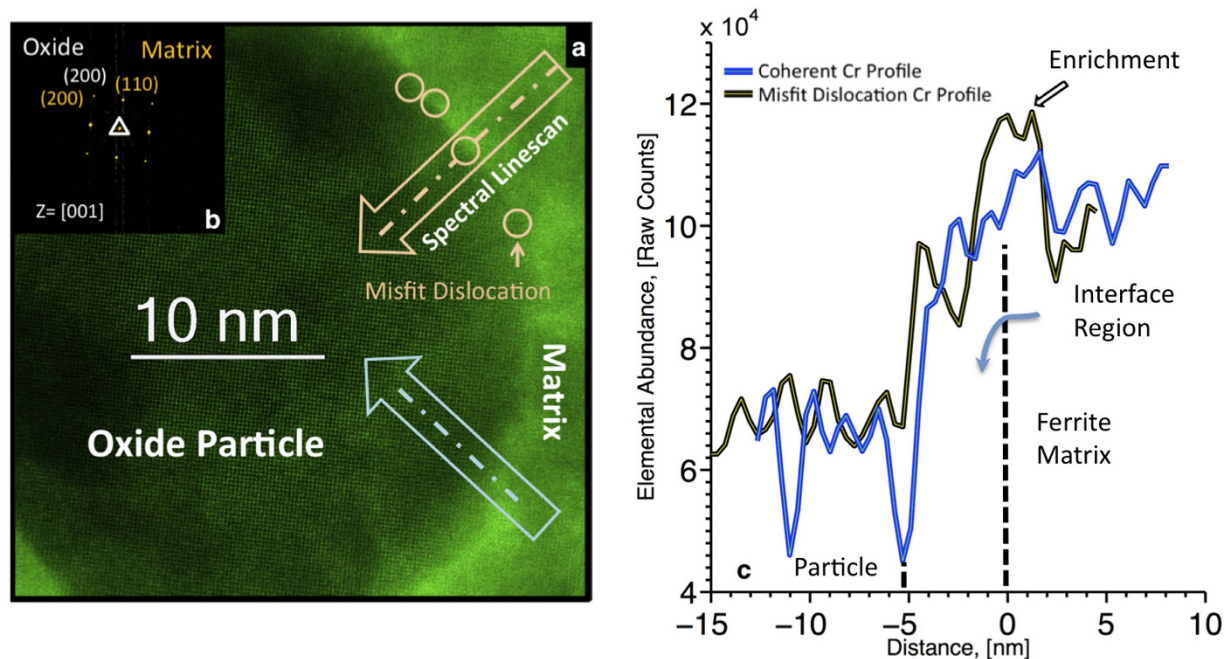
Figure 4. (**a**) STEM HAADF imaging was performed for an embedded $YAl_xCr_{1-x}O_3$ particle within a surrounding ($Fe_{0.78\pm0.04}$, $Al_{0.06\pm0.03}$, $Cr_{0.16\pm0.02}$) matrix that was oriented to the [001] zone axis, where we resolve (**b**) an out-of-plane $[200]_{matrix}||[200]_{oxide}$ and in-plane $(110)_{matrix}||(110)_{oxide}$ orientation relationship based on selected area Fast-Fourier transforms. (**c**) STEM-EELS chromium elemental line scans through a MD and in a coherent terrace was performed. Comparing the two chromium profiles reveals relative differences in chromium content at the dislocation as compared to the coherent terrace. Due to the 3-D morphology of the geometry, we have added the vertical lines to demarcate the interface region in Fig. 4c.

the preferential sites for solute segregation cannot be obtained from these thermodynamic models, requiring more elaborate electronic structure calculations as presented in this work. Moreover, these thermodynamic models do not directly take into consideration the misfit dislocation structure at internal interfaces. Nonetheless, the ability to predict solute segregation tendencies to metal/oxide interfaces is an effective first-step towards understanding the formation of secondary phases at interfaces[2,14,30,31]. Based on our results, it is expected that the tendency to form chemically sharp interfaces is enhanced if the matrix or solute has a lower oxide forming tendency than the cation in the oxide. For example, the propensity to form chemically sharp interface is improved if the oxide cation is aluminum[32], as aluminum has one of the highest oxide forming tendencies[19]. Further, our results indicate that other factors besides misfit dislocations, such as orientation relationship (OR) in polycrystalline systems, can lead to variations in oxygen content and thus segregation to different interfaces. Finally, we note that our predicted segregation behavior at metal/oxide interfaces assumes that the segregation of solutes to the interface is not limited by kinetics. However, in many cases, the final segregation profile may be limited by kinetics, depending on the experimental conditions. Further, other factors such as co-segregation of different alloying elements, solute-solute interaction in concentrated alloys, and precipitation of solutes in the bulk matrix can also change the predicted segregation behavior. Nonetheless, our results provide new insight into the intrinsic thermodynamic segregation tendency of solutes to oxygen-bearing interfaces, a first but necessary step toward understanding solute segregation behavior in more complex scenarios.

We expect that these new insights into solute segregation behavior at semi-coherent metal/oxide interfaces can be extended to other metal/ceramic systems (metal/carbide and metal/nitride) as these interfaces also exhibit non-uniform segregation of solutes between the misfit region and the terraces[33], a consequence of large chemical contributions towards segregation[34]. However, in some cases (e.g. metal/carbide) other factors, such as covalency, may also be important. To summarize, this new understanding will change how segregation at semi-coherent metal/oxide interfaces should be modeled and understood.

Methods

Electronic Structure Calculations. For the electronic structure calculations we created a bi-layer supercell consisting of three layers each of iron and yttria using the experimentally observed orientation relationship (OR) at the interface of $[001]Fe||[100]Y_2O_3$ and $(010)Fe||(011)Y_2O_3$[35]. The (110) termination of Y_2O_3 is non-polar and thus an ideal termination is favored. Other surfaces would require more extensive investigations of surface stoichiometry/reconstructions[36]. The bi-layer supercell for the electronic structure calculations consisted of three layers each of iron (a total of 165 atoms with 55 atoms in each

layer) and yttria (a total of 180 atoms with Y:O = 2:3). The top iron and bottom yttria layer are in contact with a vacuum layer of 7.25 Å. These two layers were kept frozen to replicate the bulk crystal and the interface is assumed to be atomically flat. Yttria layers are strained by -1.1% and -4.6% in the in-plane x and y direction respectively, to both capture the coherency strain between the two materials as well as to minimize the cell dimensions to make the calculations tractable. In addition to the misfit dislocation discussed in the text (with a line direction perpendicular to y), we also observe a misfit dislocation with a line direction that is perpendicular to x, accommodating the misfit between the two crystals in that direction. In contrast to the first misfit dislocation, which has a local metal/oxygen ratio greater than 1, for the second misfit dislocation the local metal/oxygen ratio is less than 1: in the x direction of the simulation cell there are eleven columns of iron for every twelve columns of oxygen. We see no great changes in chemistry or defect structure between the coherent and the misfit region for this second misfit dislocation; because of this, the behavior of this misfit dislocation is not emphasized in this manuscript. Thus, the solute segregation behavior we discuss above is sensitive to the nature of the given dislocation i.e. whether the relative extra half plane is on the metal side (dislocation line perpendicular to the y direction in our system) or on the oxide side (dislocation line perpendicular to the x direction). Further details of these calculations can be found elsewhere[16].

All the electronic structure calculations were performed using density functional theory (DFT) as implemented in the Vienna *ab-initio* Simulation Package (VASP)[20,21], using the projector augmented wave[37] method with a plane wave cut-off of 450 eV. All calculations were spin polarized using the Perdew–Burke–Ernzerhof (PBE)[38] parameterization of the generalized gradient approximation (GGA) for the exchange–correlation potential. Further, the Monkhorst-Pack scheme was utilized for Brillion zone sampling with a $1 \times 1 \times 1$ k-point mesh. The maximum force on every relaxed atom was converged to $0.05\,eVA^{-1}$ for all calculations.

Experimental Analysis. To validate the predicted Cr segregation tendencies, scanning transmission electron microscopy (STEM) high angle annular dark field (HAADF) imaging was performed on a nano-structured ferritic alloy (K3 with composition Fe-16Cr-4Al-2W-0.3Ti-0.3Y2O3) using a probe-corrected FEI Titan operated at 300 kV. STEM-based EELS was utilized to track the Cr^L and Fe^L near edge fine structures and their relative abundances with the best achievable spatial and energy resolution beyond 18 mrad collection half angles giving an energy resolution defined by the full-width half-maximum of the zero-loss peak of 1.1 eV or better. The acquisition time to resolve the near edge fine structure was performed over a series of consecutive sub-second exposures. Details of the acquisition are explained elsewhere[39]. Similar STEM-EELS approach was also used to perform chemical profiling at hetero-interfaces in our recent published work[40–42].

To observe the oxide and matrix interface with atomic resolution, the orientation relationship of the interface was first determined to be, using STEM, out-of-plane $[200]_{matrix} \| [200]_{oxide}$ and in-plane $(110)_{matrix} \| (110)_{oxide}$ orientation relationships (OR), which was confirmed based on the collected selected area diffraction of the same sample area. Later, STEM-HAADF image was acquired of the particle and matrix resolving a nearly coherent interface. Following imaging, STEM-EELS point-point linescans resolving the chemical profiles for Cr and Fe were performed traversing an interfacial dislocation and a coherent interface patch, respectively.

References

1. Stoneham, A. M. & Tasker, P. W. Metal non-metal and other interfaces - the role of image interactions. *J. Phys. C* **18,** L543–L548 (1985).
2. Meyerheim, H. L. *et al.* Geometrical and compositional structure at metal-oxide interfaces: MgO on Fe(001). *Phys. Rev. Letts.* **87,** 076102 (2001).
3. Johansson, S. A. E., Christensen, M. & Wahnstrom, G. Interface energy of semicoherent metal-ceramic interfaces. *Phys. Rev. Letts.* **95,** 226108 (2005).
4. Yanhui, W. & Diyong, W. The experimental research for production of hydrogen from n-octane through partially oxidizing and steam reforming method. *Int. J. Hydrogen Energy* **26,** 795–800 (2001).
5. Odette, G. R., Alinger, M. J. & Wirth, B. D. Recent developments in irradiation-resistant steels. *Annu. Rev. Mater. Res.* **38,** 471–503 (2008).
6. Wang, X. G., Smith, J. R. & Evans, A. Fundamental influence of C on adhesion of the Al2O3/Al interface. *Phys. Rev. Letts.* **89,** 286102 (2002).
7. Hou, P. Y. Segregation phenomena at thermally grown Al(2)O(3)/alloy interfaces. *Annu. Rev. Mater. Res.* **38,** 275–298 (2008).
8. De Hosson, J. T. M., Goren, H. B., Kooi, B. J. & Vitek, V. Metal-ceramic interfaces studied with high-resolution transmission electron microscopy. *Acta Mater.* **47,** 4077–4092 (1999).
9. Doi, T. *et al.* Analysis of Cu segregation to oxide-metal interface of Ni-base alloy by HX-PES. *Surf. Interface Anal.* **40,** 329–333 (2008).
10. Benedek, R., Minkoff, M. & Yang, L. H. Adhesive energy and charge transfer for MgO/Cu heterophase interfaces. *Phys. Rev. B* **54,** 7697–7700 (1996).
11. Benedek, R. *et al.* First principles simulation of a ceramic/metal interface with misfit. *Phys. Rev. Letts.* **84,** 3362–3365 (2000).
12. Jarvis, E. A. A. & Carter, E. A. An atomic perspective of a doped metal-oxide interface. *J. Phys. Chem. B* **106,** 7995–8004 (2002).
13. Sebastian, J. T. *et al.* Subnanometer three-dimensional atom-probe investigation of segregation at MgO/Cu ceramic/metal heterophase interfaces. *Ultramicroscopy* **89,** 203–213 (2001).
14. Mogck, S., Kooi, B. J. & De Hosson, J. T. Analysis of Gibbsian segregation at heterophase Cu-MnO interfaces. *Int. Sci.* **12,** 39–56 (2004).

15. Sebastian, J. T., Assaban, A., Seidman, D. N., Kooi, B. J. & De Hosson, J. T. M. A subnanoscale investigation of Sb segregation at MnO/Ag ceramic/metal interfaces. *Int. Sci.* **9,** 199–211 (2001).
16. Choudhury, S., Morgan, D. D. & Uberuaga, B. P. Massive Interfacial Reconstruction at Misfit Dislocations in Metal/Oxide Interfaces. *Sci. Rep.* **4,** 6533; doi: 10.1038/srep06533 (2014).
17. Isheim, D. & Seidman, D. N. Nanoscale studies of segregation at coherent heterophase interfaces in alpha-Fe based systems. *Surf. Interface Anal.* **36,** 569–574 (2004).
18. Seidman, D. N. Subnanoscale studies of segregation at grain boundaries: Simulations and experiments. *Annu. Rev. Mater. Res.* **32,** 235–269 (2002).
19. Wernick, I. K. & Themelis, N. J. Recycling metals for the environment. *Annu. Rev. Energy Environ.* **23,** 465–497 (1998).
20. Kresse, G. & Furthmuller, J. Efficient iterative schemes for ab initio total-energy calculations using a plane-wave basis set. *Phys. Rev. B* **54,** 11169–11186 (1996).
21. Kresse, G. & Hafner, J. Abinitio molecular-dynamics for liquid-metals. *Phys. Rev. B* **47,** 558–561 (1993).
22. Zhang, W., Smith, J. R., Wang, X. G. & Evans, A. G. Influence of sulfur on the adhesion of the nickel/alumina interface. *Phys. Rev. B* **67,** 245414 (2003).
23. Leslie, W. C. Iron and its dilute substitutional solid-solutions. *Metall. Trans.* **3,** 5–26 (1972).
24. Williams, C. A., Unifantowicz, P., Baluc, N., Smith, G. D. W. & Marquis, E. A. The formation and evolution of oxide particles in oxide-dispersion-strengthened ferritic steels during processing. *Acta Mater.* **61,** 2219–2235 (2013).
25. Williams, C. A., Marquis, E. A., Cerezo, A. & Smith, G. D. W. Nanoscale characterisation of ODS-Eurofer 97 steel: An atom-probe tomography study. *J. Nucl. Mater.* **400,** 37–45 (2010).
26. Finnis, M. W. The theory of metal-ceramic interfaces. *J. Phys. Condens. Matter.* **8,** 5811–5836 (1996).
27. Eremeev, S. V., Nemirovich-Danchenko, L. Y. & Kul'kova, S. E. Effect of oxygen vacancies on adhesion at the Nb/Al2O3 and Ni/ZrO2 interfaces. *Phys. Solid State* **50,** 543–552 (2008).
28. Hume-Rothery, W. *Atomic Theory for Students of Metallurgy.* fifth edn, (The Institute of Metals, London, 1969).
29. Venus, D. & Heinrich, B. Interfacial mixing of ultrathin Cr films grown on an Fe whisker. *Physical Review B* **53,** R1733–R1736 (1996).
30. Derby, B., Xiao, P. & Webster, J. Neutron reflection studies of titanium segregation to metal-ceramic interfaces. *Physica B* **248,** 304–309 (1998).
31. Luches, P. *et al.* Iron oxidation, interfacial expansion, and buckling at the Fe/NiO(001) interface. *Phys. Rev. Letts.* **96,** 106106 (2006).
32. Evans, A. G., Hutchinson, J. W. & Wei, Y. Interface adhesion: Effects of plasticity and segregation. *Acta Mater.* **47,** 4093–4113 (1999).
33. Isheim, D., Siem, E. J. & Seidman, D. N. Nanometer-scale solute segregation at heterophase interfaces and microstructural evolution of molybdenum nitride precipitates. *Ultramicroscopy* **89,** 195–202 (2001).
34. Siegel, D. J., Hector, L. G. & Adams, J. B. Adhesion, stability, and bonding at metal/metal-carbide interfaces: Al/WC. *Surf. Sci.* **498,** 321–336 (2002).
35. Inkson, B. J. & Threadgill, P. L. in *High-Temperature Ordered Intermetallic Alloys Vii* Vol. 460 *Materials Research Society Conference Proceedings* (eds C. C. Koch, C. T. Liu, N. S. Stoloff, & A. Wanner) 767–772 (1997).
36. Tasker, P. W. The stability of ionic crystal surfaces. *J. Phys. C: Solid State Phys.* **12,** 4977- 4984 (1979).
37. Blochl, P. E. Projector augmented-wave method. *Physical Review B* **50,** 17953–17979 (1994).
38. Perdew, J. P., Burke, K. & Ernzerhof, M. Generalized gradient approximation made simple. *Phys. Rev. Letts.* **77,** 3865–3868 (1996).
39. Aguiar, J. A., Reed, B. W., Ramasse, Q. M., Erni, R. & Browning, N. D. Quantifying the low-energy limit and spectral resolution in valence electron energy loss spectroscopy. *Ultramicroscopy* **124,** 130–138 (2013).
40. Aguiar, J. A. *et al.* Linking interfacial step structure and chemistry with locally enhanced radiation-induced amorphization at oxide heterointerfaces. *Adv. Mater. Interfaces* **1,** 1300142 (2014).
41. Aguiar, J. A. *et al.* Orientation-specific amorphization and intercalated recrystallization at ion-irradiated SrTiO₃/MgO interfaces. *J. Mater. Res.* **29,** 1699–1710 (2014).
42. Rama Krishnan, P. S. S. *et al.* Mapping strain modulated electronic structure perturbations in mixed phase bismuth ferrite thin films. *J. Mater. Chem. C* **3,** 1835–1845 (2015).

Acknowledgements

Author Contributions

S.C. performed all the electronic structure calculations. B.P.U. set up the initial supercell structure. S.C. and B.P.U. analyzed the electronic structure data. A.M. provided input in relating segregation energy and thermodynamic models. J.A.A. performed the experiments while M.J.F. and L.L.H. directed the experimental research. S.C. prepared the initial draft of the manuscript, while all the authors have contributed to the discussion of results and commented on the manuscript.

Additional Information

Competing financial interests: The authors declare no competing financial interests.

How to cite this article: Choudhury, S. *et al.* Non-uniform Solute Segregation at Semi-Coherent Metal/Oxide Interfaces. *Sci. Rep.* **5**, 13086; doi: 10.1038/srep13086 (2015).